JMEPEG (2010) 19:1248–1255
DOI: 10.1007/s11665-010-9626-0

1059-9495/$19.00

Surface Integrity in Grinding Medium Carbon Steel with Miniature Electroplated Monolayer cBN Wheel

Meghanshu Vashista, Shobhit Kumar, Amitava Ghosh, and Soumitra Paul

(Submitted January 13, 2009; in revised form December 17, 2009)

An experimental study was undertaken to investigate the role of process parameters on grindability of medium carbon steel with particular emphasis on surface integrity. Grinding with miniature monolayer electroplated cBN wheels provided compressive residual stress throughout the experimental domain unlike conventional grinding. This can be attributed to desirable temperature control as the wheel takes away substantial part of grinding heat flux owing to its better thermal conductivity. Micromagnetic or Barkhausen Noise (BN) parameters correlated linearly with the residual stress indicating its applicability in assessing surface integrity of cBN ground products. Increase in maximum grit depth of cut (h_m) provided more grain elongation and surface hardness due to more chip load during chip formation.

Keywords Barkhausen Noise, electroplated cBN grinding wheel, grindability, residual stress, surface integrity

1. Introduction

Grinding is primarily a finishing operation, though it can also be used for bulk material removal as in creep feed grinding and high efficiency deep grinding. Grinding is characterized by high specific energy requirement, high grinding zone temperature (Ref 1) and tensile residual stresses on the ground component (Ref 2). The surface integrity can be really poor if the grinding parameters are not chosen judiciously (Ref 3). Use of superabrasive grinding wheel, particularly cBN, tends to improve surface integrity. cBN grinding wheel can be conventionally bonded or it can as well be monolayer (Ref 2). In recent years, monolayer cBN wheels are being manufactured using galvanic or electroplating (Ref 2) or brazing route (Ref 4). Though there has been report of improved surface integrity in case of superabrasive grinding but very limited information could be obtained on monolayer miniature cBN wheel. Such wheels are primarily used for internal grinding. Monolayer wheel typically produces rougher surfaces. Ghosh and Chattopadhyay (Ref 5) investigated the beneficial effect of touch dressing on miniature monolayer cBN wheel. Similarly they have reported beneficial effect of TiN (titanium nitrate) coating in improving the performance of such wheels (Ref 6). Similar wheels have also been used in studying grindability of super alloy (Ref 7). A handful of researchers have employed Barkhausen Noise Analysis (BNA) technique for assessment of surface integrity. Comley et al. (Ref 8) estimated the residual stress using Barkhausen Noise intensity while studying the effectiveness of high efficiency deep grinding for production of automotive crankshaft. Gupta et al. (Ref 9) investigated surface integrity aspects of ground bearing steel using BNA technique.

But no work could be located on effectiveness of monolayer miniature cBN wheels in controlling surface integrity using BNA technique while grinding medium carbon steel. This paper, thus, attempts to bridge the gap by studying the effect of grinding parameters on surface integrity. A statistically designed experimental study combined with regression analysis has been undertaken on surface grinding of medium carbon steel with electroplated miniature cBN grinding wheel. Full factorial design with three factors at two levels is used in this investigation for prediction of surface integrity. The objective is to reveal the main effect of three process parameters, namely

Meghanshu Vashista, Shobhit Kumar, Amitava Ghosh, and **Soumitra Paul**, Mechanical Engineering Department, Indian Institute of Technology Kharagpur, Kharagpur, India. Contact e-mail: meghanshu@mech.iitkgp.ernet.in.

Nomenclature

V_c	grinding velocity
V_w	work speed
a	downfeed
h_m	maximum grit depth of cut
θ_m	rise in grinding temperature
q_w	heat flux entering the workpiece
L_c	contact length between grinding wheel and workpiece
K	thermal conductivity
K_g	thermal conductivity of grit
ρ	density
c	specific heat
β_w	thermal property of workpiece = $\sqrt{K\rho c}$
q_t	total heat flux
R_{ch}	ratio of heat flux partitioning to the grinding chips
R_{wg}	workpiece-wheel partition ratio
r_o	effective contact radius of the abrasive grains (taken as 10 μm for sharp wheel)
U_g	specific grinding energy
T_{mp}	melting point of workpiece material
F_t	tangential force
F_n	normal force

wheel speed (V_c), work speed (V_w) and downfeed (a), on surface integrity to judge the performance of a monolayer grinding wheel in grinding medium carbon steel.

2. Details of Experiments

2.1 Design of Experiment

To investigate the effect of grinding parameters, namely V_c, V_w and a, on different grindability characteristics, particularly surface integrity, experiments were conducted using statistical design of experiment. Full factorial experiments with three parameters (factors) at two levels were undertaken with five central points (Ref 10). Table 1 shows the levels of grinding parameters. The chosen combination of process parameters is suitable for grinding of AISI 1060 steel within the constraints of the machine tool and the combinations well represents the surface grinding with super abrasive wheel. These parameters have been coded with logarithmic coding as given next:

$$x_1 = \frac{\ln(V_c) - \ln(35)}{\ln(41) - \ln(35)} \quad \text{(Eq 1)}$$

$$x_2 = \frac{\ln(V_w) - \ln(1.9)}{\ln(2.5) - \ln(1.9)} \quad \text{(Eq 2)}$$

$$x_3 = \frac{\ln(a) - \ln(14)}{\ln(20) - \ln(14)} \quad \text{(Eq 3)}$$

where V_c is the grinding velocity in m/s, V_w the work speed in m/min, and a is the downfeed in μm.

Table 2 shows the design matrix consisting of 13 trials. Such procedure enabled development of first-order empirical models correlating grindability characteristics with the three grinding parameters through regression analysis as given next:

$$\ln Y = b_0 + b_1 x_1 + b_2 x_2 + b_3 x_3$$

where ln Y is the natural log of any grindability characteristics like residual stress, b_0 the constant, b_1 the coefficient of coded value of V_c, b_2 the coefficient of coded value of V_w, b_3 the coefficient of coded value of a, x_1, x_2, x_3 the coded value of V_c, V_w, and a as per Eq 1, 2, and 3.

Table 1 Level of independent variables

Levels	Low	Center	High
Coding	−1	0	1
Wheel speed (V_c), m/s	30	35	41
Work speed (V_w), m/min	1.5	1.9	2.5
Infeed (a), μm	10	14	20

Table 2 Experimental conditions

					Coding		
Trial no.	Rank	V_c, m/s	V_w, m/min	a, μm	x_1	x_2	x_3
1	II	41	2.5	20	1	1	1
2	VIII	41	1.5	20	1	−1	1
3	IV	30	2.5	20	−1	1	1
4	VI	30	1.5	20	−1	−1	1
5	I	41	2.5	10	1	1	−1
6	VII	41	1.5	10	1	−1	−1
7	III	30	2.5	10	−1	1	−1
8	V	30	1.5	10	−1	−1	−1
9	IX	35	1.9	14	0	0	0
10	X	35	1.9	14	0	0	0
11	XI	35	1.9	14	0	0	0
12	XII	35	1.9	14	0	0	0
13	XIII	35	1.9	14	0	0	0

2.2 Experimental Details

Thirteen specimens were prepared from AISI 1060 steel. The reason for choosing this steel is that it contains medium (0.6%) carbon percentage and it is representative of the typical behavior of many carbon and alloy steels so that observations developed can be reasonably applied to many steels. All specimens are having same rectangular shape [$75^L \times 10^H \times 7^W$ mm]. Grinding tests were realized in plunge surface grinding mode using high-speed spindle (20,000-66,000 rpm). Electroplated cBN grinding wheel (wheel diameter = 15 mm, face width = 10 mm, shank diameter = 8 mm, shank length = 15 mm) was submitted to grinding of specimens under dry environment. A high-resolution piezoelectric type (make-KISTLER Instrumente AG Winterthur Switzerland, model: 9254) dynamometer along with two charge amplifier (make-KISTLER Instrumente AG Winterthur Switzerland, model: 5011B10) and a data acquisition system have been used in this work for force measurement. Under each test condition, eight passes were taken and tangential and normal forces were measured for all these passes. Grinding cycle consists of three parts: spark-in, steady state, and spark-out. Eight passes were taken so that the steady state can be reached (after spark-in state), which was typically achieved within 2 to 3 passes. Average of grinding forces obtained during steady state grinding was considered for analysis. Surface profile of ground surface, thus produced, was traced by 2-D profilometer (Model: Surtronic 3+ make: Taylor Hobson, with cut off: 0.8 mm) in the transverse direction.

The BN measurements were carried out using the commercially available μscan/Rollscan-300 system supplied by Stresstech, Finland. A flat surface probe with a BN signal pick-up coil at the center was used to apply the excitation magnetic field and to receive the BN signal. Ground samples were cleaned before measurement by isopropyl alcohol in order not to disturb the BN signal which is surface dependent. BN measurements were carried out with a 100 Hz excitation frequency magnetic field and 3.5 V magnetizing voltage. The frequency of filter was adjusted for maximum sensitivity at a near surface depth where maximum change in surface integrity was expected. For each sample, five observations were taken and analyzed by μscan software to register the BN parameters. Root mean square (rms) and peak value of BN signal was selected for analysis. Average value of observed BN parameters was considered for investigating the effect of grinding process parameters.

It was necessary to establish the reference to identify the level of residual stress. So ground samples were also characterized by using x-ray diffraction technique (XRD). Absolute residual stress magnitudes were determined along the grinding direction using Philips X'pert x-ray diffractometer, Philips X'pert Data Collector and Philips X'pert stress software. Pearson VII technique (Ref 11) was used to calculate the peak

position on the diffracted intensity plots. The central area of ground samples was taken as the location for both BN and XRD measurement.

Ground samples were sectioned perpendicular to and along the grinding direction. These were subsequently hot moulded in specimen mount press (Buehler, USA) by phenolic resin powder, along with dummy samples for maximum edge retention. Moulded samples were polished on different emery papers with successively fine grit of mesh of 220, 400 and 600 followed by cloth polishing with Al_2O_3 paste and finally diamond polished on auto-disc polishing machine (Struers LaboForce-3) until a mirror-like surface was obtained, cleaned using lab detergent, and then etched for about 10 s using 5% nital solution. The samples were immediately rinsed using running water and dried using hot air for observation of cross and longitudinal section of the ground surface under an inverted metallurgical optical microscope (Olympus, Japan).

Microhardness (HV) of the ground surface and subsurface was examined with microhardness tester, LM 700 (Leco, USA). Microhardness tests were carried out with 50 g load and 10 s dwell time on the cross sections of ground samples with a Vicker indenter from a depth of 25 μm. This is a practical limitation because of loss of material constraint at positions closer to the surface, and a limit of 2.5 times the indentation diagonal as recommended by ASTM standard E 92. For each sample, five hardness measurements were undertaken at this depth below the edge but well spaced to avoid interference between each indent. Average value of these five measurements was considered for analysis.

2.3 Estimation of Grinding Temperature

The estimation of temperature has been carried out using the model proposed by Rowe (Ref 12). The grinding temperature rise is estimated in dry environment by the following equation:

$$\theta_m = 1.13\frac{q_w}{\beta_w}\sqrt{\frac{L_c}{V_w}} \quad \text{(Eq 4)}$$

The q_w again can be estimated by

$$q_w = \eta q_T \quad \text{(Eq 5)}$$

where

$$\eta = R_{wg}(1 - R_{ch}) \quad \text{(Eq 6)}$$

where (Ref 13)

$$R_{wg} = \left[1 + \frac{0.97K_g}{\beta_w \sqrt{r_0 V_c}}\right]^{-1} \quad \text{(Eq 7)}$$

and (Ref 14)

$$R_{ch} = \frac{\rho_w C_w T_{mp}}{U_g} \quad \text{(Eq 8)}$$

By using these equations and heat partition ratio mentioned above, the grinding temperature (θ_m) can be estimated. Table 3 enlists the thermal properties of work (medium carbon steel) and cBN considered to estimate the grinding temperature (www.matweb.com). Edge radius (r_0) of 10 μm has been used in the present work as reported earlier for cBN grits (Ref 15).

3. Results and Discussion

Table 4 shows the experimental results like tangential force, normal force, surface roughness, residual stress, BN parameters and microhardness of ground surface for different combination of process parameters. The details of parametric combination are given in Table 2.

Serial numbers 9 to 13 in Table 4 exhibit the repeatability and robustness of the experiment procedure and different responses. For example, tangential force varies within a close range of 3.26 N to 3.5 N, indicating the repeatability.

Regression analysis has been adopted to develop empirical relations between responses and grinding parameters, namely V_c, V_w and a. Adequacy of the models and significance of

Table 3 Thermal properties of work and superabrasive

Melting point, T_{mp} (work), °C	Density, ρ (work), kg/m^3	Specific heat, c (work), J/kg °C	Thermal conductivity, K (work), W/m · K	Thermal conductivity, K (cBN), W/m · K
1530	7850	475	44.5	240

Table 4 Experimental results

Trial no.	F_t, N	F_n, N	Residual stress, MPa	BN (rms)	BN (peak)	Roughness R_a, μm	Microhardness $HV_{0.05}$
1	5.02	8.94	−76	194	277	4.68	290
2	3.06	5.48	−140	185	266	4.39	221
3	5.88	9.64	−124	182	249	4.74	301
4	3.68	6.14	−240	158	220	4.57	287
5	3.25	5.62	−102	192	282	4.42	229
6	2.28	3.97	−224	172	242	4.13	192
7	4.5	7.15	−226	181	253	4.55	279
8	2.76	4.64	−255	132	185	4.15	207
9	3.26	5.44	−121	181	248	4.46	237
10	3.26	5.51	−127	168	239	4.53	262
11	3.32	5.54	−159	173	240	4.55	269
12	3.37	5.63	−150	177	246	4.53	250
13	3.5	5.8	−143	179	248	4.49	241

Table 5 ANOVA for tangential force (F_t) $F_t = 6.986\,V_c^{-0.6754}V_w^{0.822}a^{0.449}$ correlation coefficient = 0.9516

	Degree of freedom	Sum of square	Mean of square	F_{ratio} (calc.)	F_{ratio}(a) (table)
Total	12	0.7424	0.0619		
Regression	3	0.7065	0.2355	270.6498	16.69
V_c	1	0.0923	0.0923	106.0203	21.2
V_w	1	0.4081	0.4081	469.0384	21.2
a	1	0.2061	0.2061	236.8908	21.2
Error	10	0.0359	0.0036		
Lack of fit	5	0.0324	0.0065	7.4516	15.52
Pure error	4	0.0035	0.0009		

(a) At 99% level

individual coefficients have been tested using Fisher test. Insignificance of the lack of fit has also been compared with respect to pure error using Fisher test (F-ratio, which is the ratio of mean of square of source to mean of square of pure error).

Table 5 shows the detailed ANOVA (analysis of variance) for tangential force. The ANOVA clearly indicates significance of all coefficients and insignificance of lack of fit with respect to pure error. The model is adequate indicated further by a correlation coefficient of 0.9516. The tangential force seems to increase with increase in V_w and a and reduction in V_c. Lot of manufacturing processes can be characterized by unit events. For example, electric discharge machining (EDM) is characterized by spark leading to crater formation. So sparking and crater formation is the unit event in EDM. Similarly, in grinding the unit event is chip formation due to micro-cutting by abrasive grains. This unit event is characterized by maximum unit chip thickness or maximum grit depth of cut (h_m) (Ref 16). h_m is given by

$$h_m = \left[\frac{3}{c\tan\alpha}\frac{V_w}{V_c}\sqrt{\frac{a}{d}}\right]^{1/2} \quad \text{(Eq 9)}$$

Increase in V_w and a raises h_m or chip load on a single abrasive grit. This is expected to increase tangential force. Similarly, increase in V_c leads to reduction in h_m providing less tangential force. In conventional grinding, similar effect though in different degree has been reported earlier (Ref 15). Grinding of hardened steel with vitrified bonded cBN wheel also indicated similar effects (Ref 16).

The empirical equation as given in Table 6 reveals the effect of V_c, V_w and a on normal force. The relative effect of grinding parameters on normal force is very similar to their effect on tangential force.

The dominant effect of V_c and V_w, in that order, on the force ratio is clearly noted from the empirical equation given in Table 6. Typically, the force ratio varies between 1.5 to 5 (Ref 3, 17). In superabrasive grinding, the grits are sharper than conventional abrasives. This leads to less variation in effective rake for change in downfeed from 10 to 20 μm. Thus, downfeed in the present experiment have very less effect on the force ratio. Grinding velocity affects h_m more than workspeed. Thus, its effect on the grinding ratio is also more. Previous researcher has indicated a grinding force ratio domain of 1.5 to 1.8 while grinding cemented carbide with brazed diamond wheel (Ref 18). Though the range of grinding force matches with the current investigation, but the effect of h_m on force ratio is just the opposite. At higher h_m, the effective negative rake angle is less leading to less rubbing and ploughing resulting in lower F_n/F_t. This hypothesis has clear support from previous published literature (Ref 15).

Table 6 List of empirical equations

Serial no.	Response	Empirical equation
1	Tangential force	$F_t = 6.986V_c^{-0.6754}V_w^{0.822}a^{0.449}$
2	Normal fore	$F_n = 5.23V_c^{-0.46}V_w^{0.784}a^{0.478}$
3	Force ratio	$\frac{F_n}{F_t} = 0.746V_c^{0.218}V_w^{-0.041}a^{0.027}$
4	Surface roughness	$R_a = 4.17V_c^{0.068}V_w^{0.1186}a^{0.089}$
5	Specific energy	$u_g = 55.62V_c^{0.307}V_w^{-0.108}a^{-0.521}$
6	Grinding temperature	$\theta = 11.79V_c^{0.609}V_w^{0.337}a^{0.117}$
7	Residual stress	$\sigma = -250196V_c^{-1.536}V_w^{-0.994}a^{-0.449}$
8	BN (rms)	$\text{BN (rms)} = 24.70V_c^{0.429}V_w^{0.28}a^{0.094}$
9	BN (peak)	$\text{BN (peak)} = 24.91V_c^{0.529}V_w^{0.288}a^{0.082}$
10	Microhardness	$HV_{0.05} = 473.66V_c^{0.449}V_w^{0.362}a^{0.273}$

Grinding is primarily a finishing process, thus roughness of the ground surface is important. Empirical equation relating surface roughness with process parameters as given in Table 6 reveals their effects on roughness of the ground surface. The range of roughness is in between 4 to 5 μm. This seems to be very high as very sharp cBN grits tends to produce rougher surface without plastic deformation particularly in plunge surface grinding mode, as has been reported earlier (Ref 5). Surface roughness is typically high for any combination of grinding parameter which leads to increase in h_m. The present results conform to this observation along with observation of previous researcher (Ref 16, 17).

Grinding specific energy is one of the most important responses in understanding mechanics of grinding (Ref 19). Relevant equation in Table 6 (serial number 5) indicates reduction in grinding specific energy with increase in a and V_w and reduction in V_c. Such change in grinding parameters leads to increase in h_m. Increase in h_m leads to favorable rake angle during chip formation in grinding. It also helps in reducing rubbing and ploughing. All these effects enable reduction in specific energy for any increase in h_m (Ref 15, 19). The effect of increase in V_c is more complicated. Increase in V_c leads to increase in grinding temperature and expectedly shear plane temperature. This should bring down the effective strength of the work material and specific energy. But increase in V_c also leads to increase in strain rate resulting in more effective strength of the work material and thus more specific

energy. Similar observations have also been noted by Shaw (Ref 19). In the present case, it seems the strain rate effect is predominating the temperature reduction effect. This could be attributed to possibly not very high grinding zone temperature due to use of cBN grinding wheels.

Temperature on the ground surface has been estimated as detailed in Sect 2.3. Increase in grinding parameters leads to increase in grinding temperature as has also been captured by the corresponding empirical equation in Table 6 (serial number 6). Interestingly the domain of grinding temperature for the present combination of the parameters is 140-220 °C only. Conventional grinding typically leads to much higher grinding zone temperature. On the other hand, grinding with cBN wheels provides reasonably lower grinding temperature (Ref 2). This may be attributed to two reasons. Use of cBN wheels having a thermal conductivity of 240 W/m·K enables the wheel to take away significant part of the energy. Further, the cBN grits are sharper than conventional grit material. This, in turn, provides less specific energy and thus less heat load.

Increase in a though reduces specific energy but increases the heat flux entering the workpiece. This leads to increase in grinding temperature as per Eq 4. Increase in V_w affects q_w in such a manner for the present work that it leads to increase in grinding temperature. Effect of V_c is more straight-forward as increase in V_c leads to more grinding power, more q_w and thus more grinding temperature.

Surface integrity is a combined characteristic. It incorporates responses like state of stress, microhardness, microstructure and surface roughness. Among them residual stress is one of the most important characteristics. Increase in all the grinding parameter indicates reduction in compressive residual stress as noted by the corresponding empirical equation in Table 6 (serial number 7). Interestingly the domain of residual stress is always compressive. Conventional grinding typically produces tensile residual stress, whereas cBN grinding tends to produce less tensile residual stress (Ref 20). The origin of residual stress in grinding is threefold. Any machining operation tends to induce compressive residual stress because of cutting action by the tools. Typically for a ferrous material austenitic to martensitic transformation may as well introduce transformation metallurgical stress. The third source of residual stress is typically tensile in nature which occurs due to plastic deformation of the ground surface during grinding due to rise in temperature. Increase in all grinding parameters leads to increase in temperature as indicated earlier. This increase in temperature tends to yield more tensile residual stress. Thus as a combined effect, increase in grinding parameters in the current work provided less compressive residual stress.

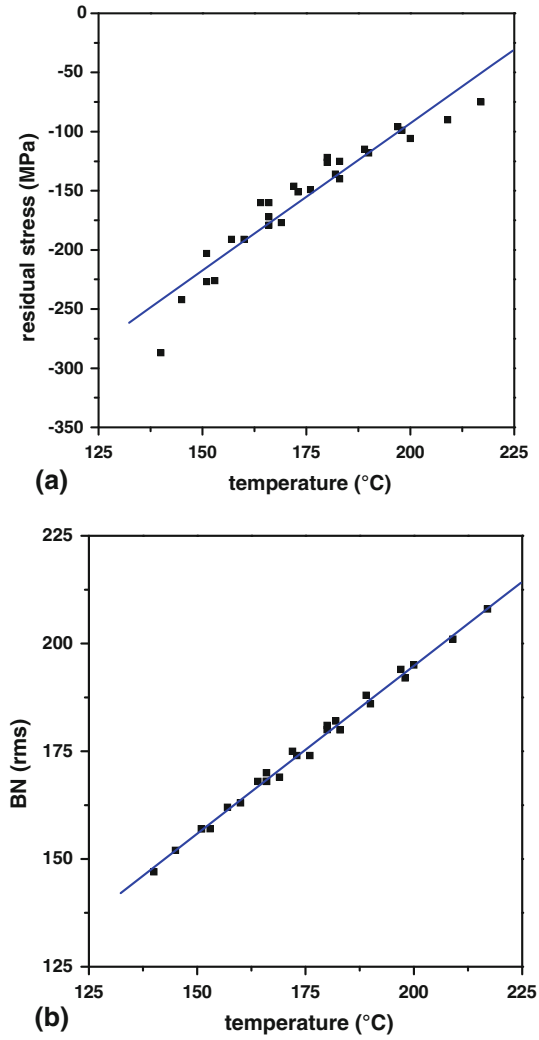

Fig. 1 Variation in residual stress and BN (rms) with temperature

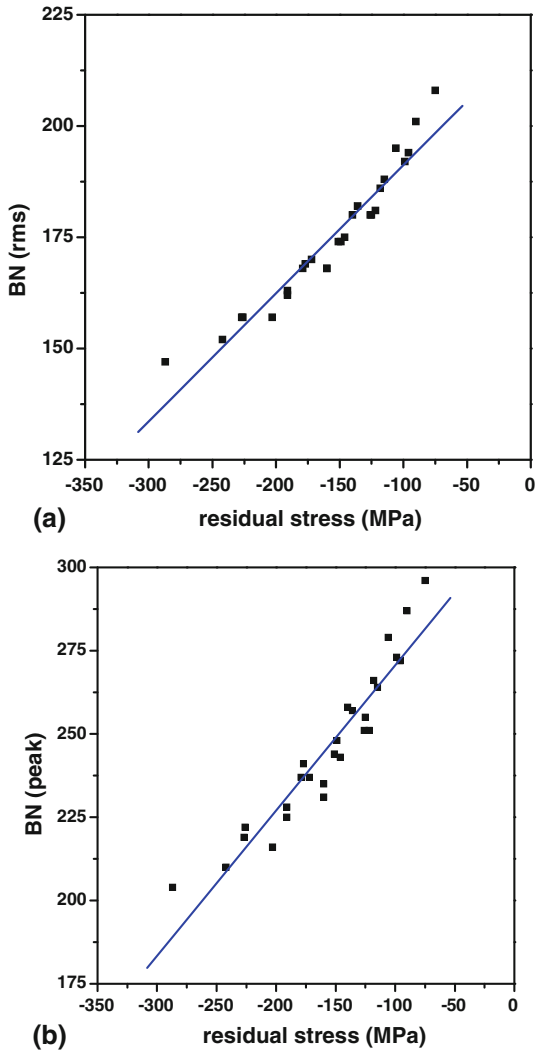

Fig. 2 Effect of residual stress on BN parameters

As has been reported earlier that measurement of residual stress using XRD technique remains a laboratory-based procedure as well time-consuming activity (Ref 20). Its only advantage is its accuracy. On the other hand, micromagnetic technique like BN analysis can be employed in the shop floor for the assessment of surface integrity. Micromagnetic response of a material however depends on not only the state of residual stress but also on hardness, grain size and surface roughness (Ref 21). Typically rms and peak value of BN are correlated with respect to surface integrity. Increase in a, V_w and V_c has provided increase in BN (rms) and BN (peak) as noted in Table 6 (serial number 8 and 9). The micromagnetic response, as characterized by BN (rms) and BN (peak), gets augmented when the compressive residual stress decreases (Ref 22). Thus, comparing equations (serial number 7, 8 and 9 in Table 6), it can be inferred that there is correlation among BN parameters and surface residual stress after grinding medium carbon steel with monolayer cBN wheel.

The residual stress in grinding increases with increase in grinding zone temperature till about 700 °C for steel (Ref 2). Figure 1 shows almost linear correlation between residual

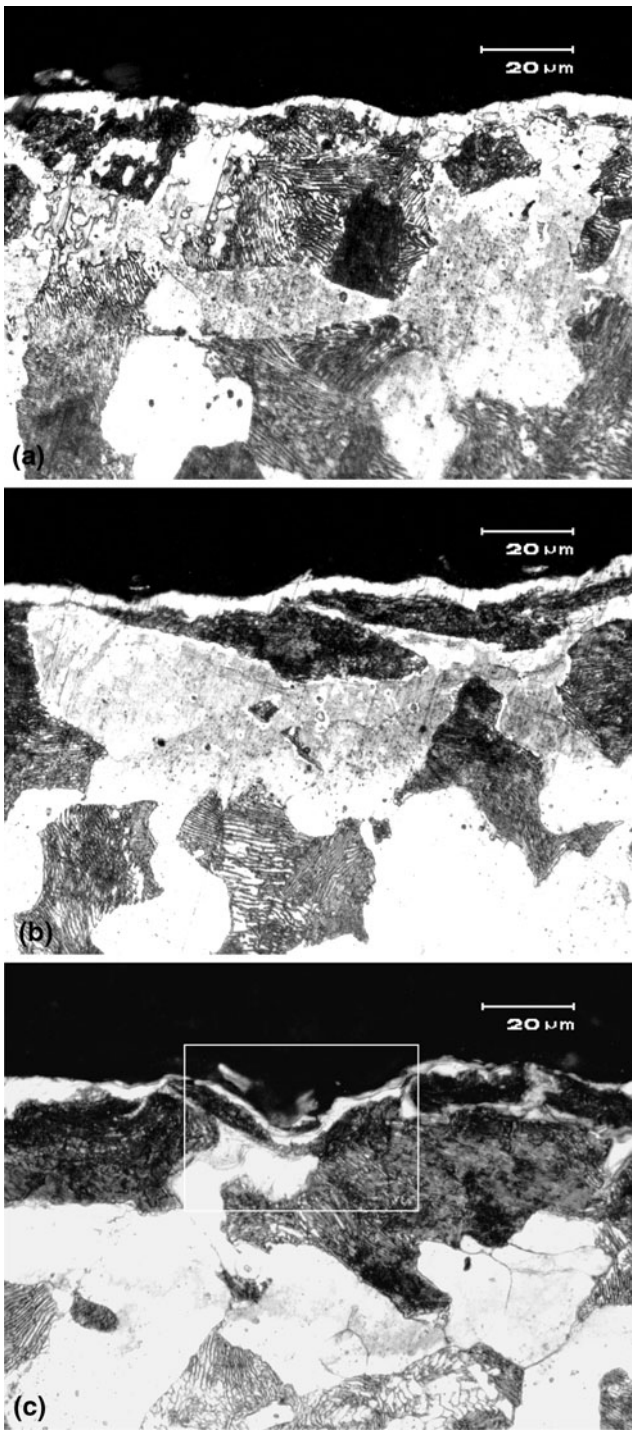

Fig. 3 Micrographs at different combination of process parameters: cross-sectional view at 500× for (a) h_m lowest, (b) h_m moderate, and (c) h_m highest

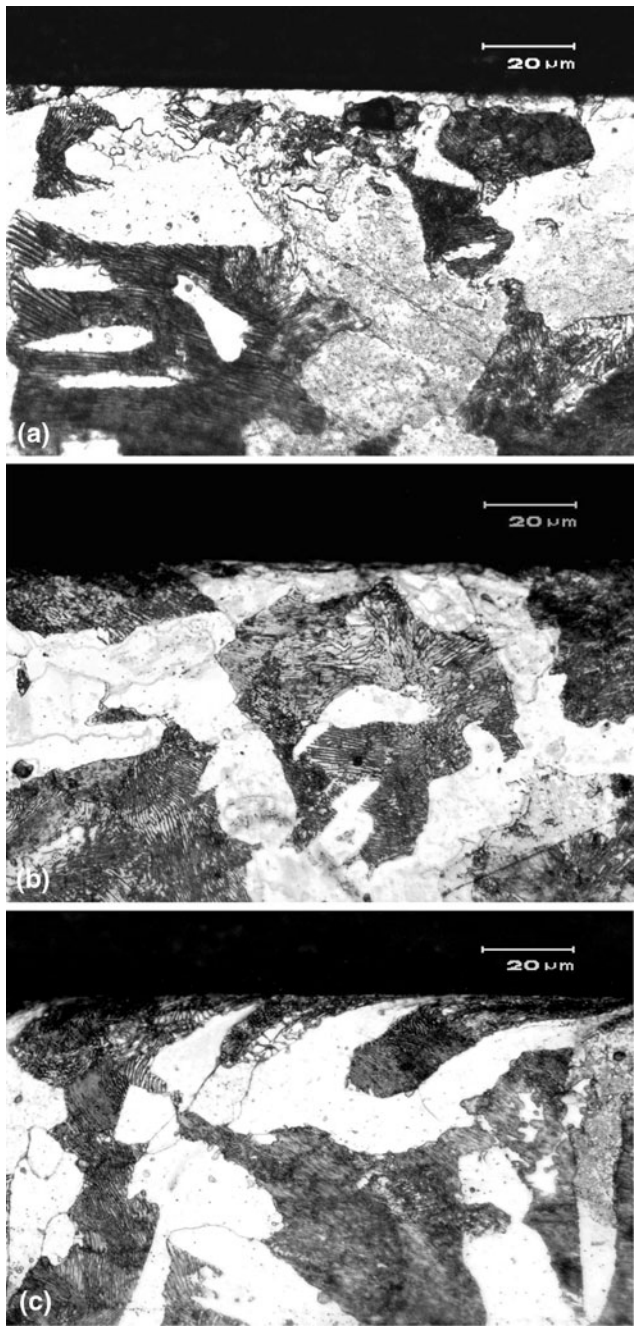

Fig. 4 Micrographs at different combination of process parameters: longitudinal section view at 500× for (a) h_m lowest, (b) h_m moderate, and (c) h_m highest

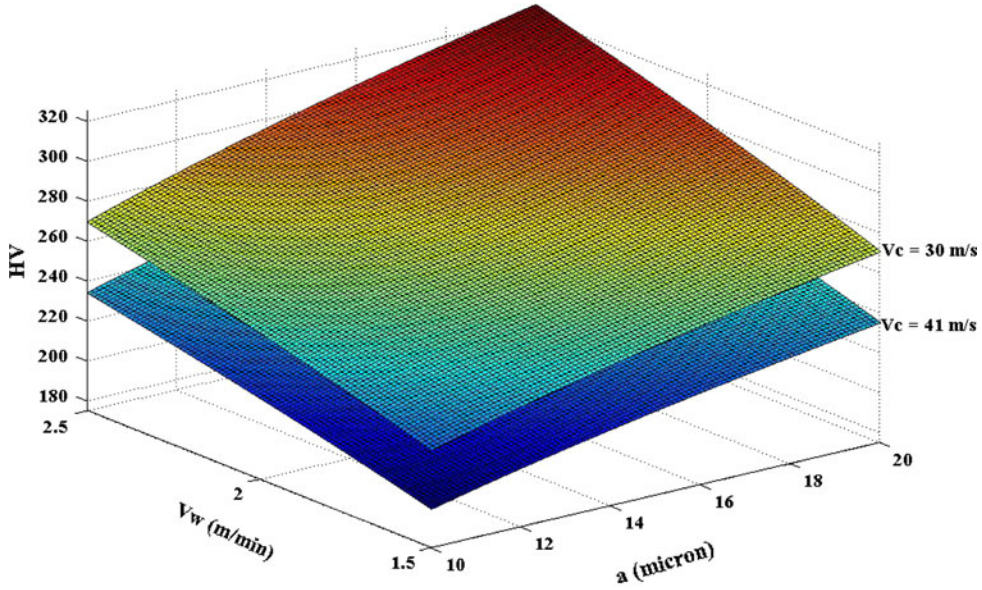

Fig. 5 Variation in surface hardness with process parameters

stress and BN (rms) with grinding temperature expectedly. With increase in grinding temperature the residual stress increases; that is, compressive residual stress decreases and thus BN (rms) increases. Figure 2 similarly shows almost linear relationship between residual stress and two of the BN parameters.

Surface integrity also incorporates properties like hardness, plastic deformation and grain refinement. Figure 3 shows the effect of maximum grit depth of cut on microstructure of the ground component. It seems as h_m increases, the action of grit producing rougher surface gets captured in the cross-sectional micrograph as indicated by white rectangle. The microstructure also reveals some grain refinement producing the classical white layer in grinding. Typically white layer is produced in conventional grinding when temperature is high. But cBN grinding also provide white layer as reported earlier (Ref 23). This could be attributed to more strain rate in cBN grinding due to higher grinding velocity (Ref 19).

Grain elongation along the grinding velocity direction does occur, indicating plastic deformation due to cutting action of the abrasive grits (Ref 24). Figure 4 shows longitudinal section of the ground component with increasing maximum grit depth of cut or chip load. Almost no grain elongation is observed till a moderate h_m is exceeded. The highest h_m in the current experimental domain does provide grain elongation over a depth of around 16 μm, indicating plastic deformation.

Such plastic deformation along with white layer formation is expected to change the hardness of the ground surface. Figure 5 clearly reveals increase in microhardness of the ground surface with increase in a, V_w and decrease in V_c, which means an increase in h_m or chip load provides more intensive cutting action by the abrasive grits leading to more increase in hardness. However, some researchers have indicated decrease in hardness with increase in tensile residual stress (Ref 25). But comparing Fig. 5 and equation of residual stress (Table 6, serial number 7), just the reverse trend is observed in the present case. Literature indicates that when the residual stress is highly tensile it dominates over grain elongation resulting in reduction in hardness. In the present work, the residual stress is primarily

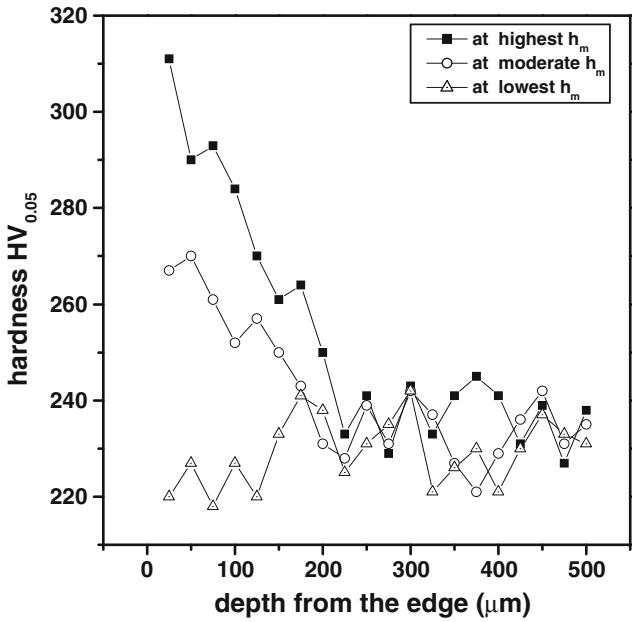

Fig. 6 Hardness profile at different combination of parameters

compressive and in the domain of −250 MPa to −50 MPa, thus grain elongation and white layer formation enhance the surface hardness. Figure 6 provides direct experimental evidence of increase in surface hardness upon grinding particularly at moderate and high h_m.

4. Conclusions

1. Grinding of medium carbon steel with miniature monolayer electroplated cBN wheel provided compressive residual stress throughout the experimental domain. This is attributed to desirable temperature control as

electroplated cBN wheel could take away substantial part of heat flux due to its higher thermal conductivity.
2. Increase in grinding parameters, namely V_c, V_w and a, reduced the compressive residual stress due to more grinding temperature at higher levels of grinding parameters.
3. Micro-magnetic response of the work material characterized by BN (rms) and BN (peak) got augmented with increase in grinding parameters.
4. Linear relationships could be established between BN parameters and state of residual stress. This enables use of BNA technique for assessing surface integrity in cBN grinding.
5. Increase in average grit depth of cut produced white layer as well as grain elongation, indicating predominant of mechanical cutting action in cBN grinding.
6. Similarly, surface hardness upon grinding increased with increasing grit depth of cut.

References

1. J.O. Outwater and M.C. Shaw, Surface Temperature in Grinding, *Trans. ASME*, 1952, **74**, p 73–86
2. S. Malkin and C. Guo, Thermal Analysis of Grinding, *Ann. CIRP*, 2007, **56**(2), p 760–782
3. S. Paul and A.B. Chattopadhyay, A Study of Effect of Cryo-cooling in Grinding, *Int. J. Mach. Tools Manuf.*, 1995, **35**(1), p 109–117
4. A.K. Chattopadhyay and H.E. Hintermann, On Performance of Brazed Single Layer cBN Wheel, *Ann. CIRP*, 1994, **43**(1), p 313–317
5. A. Ghosh and A.K. Chattopadhyay, Experimental Investigation on Performance of Touch-Dressed Single Layer Brazed cBN Wheel, *Int. J. Mach. Tools Manuf.*, 2007, **47**, p 1206–1213
6. A. Ghosh and A.K. Chattopadhyay, Performance Enhancement of Single Layer Miniature cBN Wheels Using CFUBMS-Deposited TiN Coating, *Int. J. Mach. Tools Manuf*, 2007, **47**(12–13), p 1749–1806
7. U. Teicher, A. Ghosh, A.B. Chattopadhyay, and K. Kunanz, On Grindability of Titanium Alloy by Brazed Type Monolayered Superabrasive Grinding Wheels, *Int. J. Mach. Tools Manuf*, 2006, **46**(6), p 620–622
8. P. Comley, J. Walton, T. Jin, and D.J. Stephenson, A High Material Removal Rate Grinding Process for the Production of Automobile Crankshafts, *Ann. CIRP*, 2005, **55**(1), p 347–350
9. H. Gupta, M. Zhang, and A.P. Parakka, Barkhausen Effect in Ground Steels, *Acta Metall.*, 1997, **45**(5), p 1917–1921
10. R.G. Petersen, *Design and Analysis of Experiments*, Marcel Dekker, Inc, New York, 1985, p 124
11. I.C. Noyan and J.B. Cohen, *Residual Stress—Measurement by Diffraction and Interpretation*, Springer-Verlag, New York, 1987, p 168
12. W.B. Rowe, Thermal Analysis of High Efficiency Deep Grinding, *Int. J. Mach. Tools Manuf.*, 2001, **41**, p 1–19
13. R.S. Hahn, On Nature of the Grinding Process, *Proceedings of the 3rd Machine Tool Design and Research Conference*, 1962, p 129–154
14. T. Jin, W.B. Rowe, and D. McCormach, Temperature in Deep Grinding of Finite Workpieces, *Int. J. Mach. Tools Manuf.*, 2002, **42**, p 53–59
15. S. Ghosh, A.B. Chattopadhyay, and S. Paul, Modelling of Specific Energy Requirement During High Efficiency Deep Grinding, *Int. J. Mach. Tools Manuf.*, 2008, **48**(11), p 1242–1253
16. S. Chakrabarti and S. Paul, Numerical Modelling of Surface Topography in Superabrasive Grinding, *Int. J. Adv. Manuf. Tech*., 2007. doi: 10.1007/s00170-007-1201-y
17. P. Tso and C. Lu, Study on the Grinding of P/M High Speed Steel ASP60, *Int. J. Mach. Tools Manuf.*, 1999, **39**, p 627–638
18. S. Li, J. Xu, B. Xiao, M. Yan, Y. Fu, and H. Xu, Performance of Brazed Diamond Wheel in Grinding Cemented Carbide, *Mater. Sci. Forum*, 2006, **532–533**, p 381–384
19. M.C. Shaw, Energy Conversion in Cutting and Grinding, *Ann. CIRP*, 1996, **45**(1), p 101–104
20. E. Brinksmeier, J.T. Commett, W. Konig, P. Leskovar, J. Peters, and H.K. Tonshoff, Residual Stress—Measurement and Causes in Machining Processes, *Ann. CIRP*, 1982, **31**(2), p 491–510
21. B. Karpuschewski and T. Mandrysch, Micromagnetic In-process Surface Integrity Analysis of Ground Workpieces, *Proceedings of the 1st International Conference on Barkhausen Noise and Micromagnetic Testing*, Germany, 1998, p 1–13
22. J. Gauthier, T.W. Krause, and D.L. Atherton, Measurement of Residual Stress in Steel Using Magnetic Barkhausen Noise Technique, *NDT & E Int.*, 1998, **31**(1), p 23–31
23. C. Guo, Z. Shi, H. Attia, and D. Mclntosh, Power and Wheel Wear for Grinding Nickel Alloy with Plated cBN Wheels, *Ann. CIRP*, 1999, **56**(1), p 343–346
24. T. Matsuo, H. Shibahara, and Y. Ohbuchi, Curvature in Surface Grinding of Thin Workpieces with Superabrasive Wheels, *Ann. CIRP*, 1987, **36**(1), p 231–234
25. S. Malkin, Current Trends in cBN Grinding Technology, *Ann. CIRP*, 1985, **34**(2), p 557–563